JUSTC

Article

http://justc.ustc.edu.cn

C_{60}-derived long-range ordered porous carbon as anodes for lithium-ion and sodium-ion batteries

Shengyuan Li[1*], Yizhe Wang[2*], Yanbo Zhang[1], Fei Pan[1] ✉, and Yanwu Zhu[1,2,3] ✉

[1]*Department of Materials Science and Engineering, School of Chemistry and Materials Science, University of Science and Technology of China, Hefei 230026, China;*
[2]*Hefei National Research Center for Physical Sciences at the Microscale, University of Science and Technology of China, Hefei 230026, China;*
[3]*Key Laboratory of Precision and Intelligent Chemistry, University of Science and Technology of China, Hefei 230026, China*

* These authors contributed equally to this work
✉Correspondence: Fei Pan, E-mail: feipan@ustc.edu.cn; Yanwu Zhu, E-mail: zhuyanwu@ustc.edu.cn

Graphical abstract

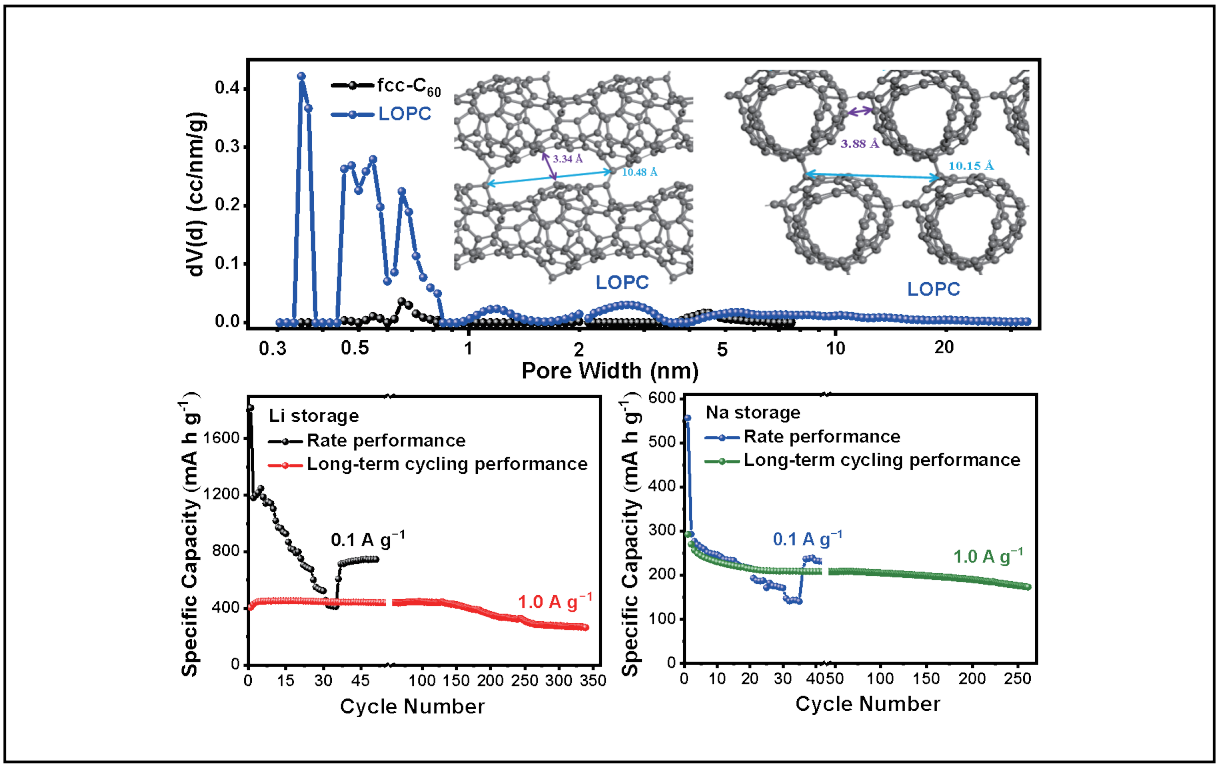

The rich ultramicropores of LOPCs as anodes for LIBs or SIBs achieve excellent rate performance and cycling stability.

Public summary

- The long-range ordered porous carbon was prepared via the electron injection method, and the cavity size of the simulated structure was in good agreement with the pore size distribution of the gas adsorption test.
- LOPC consists of sp^2-carbon-connected partially broken fcc C_{60} cages with a rich ultraporous structure and has a greater specific surface area (327.1 $m^2 \cdot g^{-1}$) than fcc C_{60} powder (14.3 $m^2 \cdot g^{-1}$).
- The electrical conductivity and structural stability of LOPC were improved, and the LOPC was used as an anode for LIBs or SIBs to achieve excellent rate performance and cycling stability.

Citation: Li S Y, Wang Y Z, Zhang Y B, et al. C_{60}-derived long-range ordered porous carbon as anodes for lithium-ion and sodium-ion batteries. *JUSTC*, **2026**, 55(0): . CSTR: 32290.14.JUSTC-2024-0115. DOI: 10.52396/JUSTC-2024-0115

JUSTC

Article

http://justc.ustc.edu.cn

C_{60}-derived long-range ordered porous carbon as anodes for lithium-ion and sodium-ion batteries

Shengyuan Li[1*], Yizhe Wang[2*], Yanbo Zhang[1], Fei Pan[1] ✉, and Yanwu Zhu[1,2,3] ✉

[1]*Department of Materials Science and Engineering, School of Chemistry and Materials Science, University of Science and Technology of China, Hefei 230026, China;*
[2]*Hefei National Research Center for Physical Sciences at the Microscale, University of Science and Technology of China, Hefei 230026, China;*
[3]*Key Laboratory of Precision and Intelligent Chemistry, University of Science and Technology of China, Hefei 230026, China*

* These authors contributed equally to this work
✉Correspondence: Fei Pan, E-mail: feipan@ustc.edu.cn; Yanwu Zhu, E-mail: zhuyanwu@ustc.edu.cn

Cite This: *JUSTC*, **2026**, 55(X): (7pp) Read Online SI Supporting Information

Abstract: The search for novel carbons has been an important research topic for developing high-performance anodes of lithium-ion batteries (LIBs) and sodium-ion batteries (SIBs). In this study, we fabricated a new carbon, long-range ordered porous carbon (LOPC), by inducing covalent bonds between face-centered cubic C_{60} (fcc C_{60}) cages in a molecular crystal via electron injection under vacuum at ~ 520 °C. The LOPC maintains the periodic lattice of the fcc C_{60} molecular crystal but has improved structural stability and electrical conductivity because of the sp^2 bonding formed between C_{60} molecules. Compared with fcc C60, which has a much greater specific surface area (327.1 $m^2 \cdot g^{-1}$), LOPC has a specific capacity of 820.9 $mA \cdot h \cdot g^{-1}$ or 292.9 $mA \cdot h \cdot g^{-1}$ as an anode for LIBs or SIBs, both of which are measured at a current density of 0.1 $A \cdot g^{-1}$. This porous yet ordered carbon may open new opportunities for anode materials in electrochemical energy storage.

Keywords: Lithium-ion batteries; sodium-ion batteries; fullerene C_{60}; electron injection; long-range ordered porous carbon
CLC number: **Document code:** A

1 Introduction

Lithium-ion batteries (LIBs) are premiere power sources that play indispensable roles in modern society owing to their advantages, such as high energy density[1]. Compared with the early use of metallic Li directly as an anode, the improved safety of current LIBs is mainly attributed to the graphite anode, which stores or releases Li ions at a relatively stable potential. However, the theoretical capacity of 372 $mA \cdot h \cdot g^{-1}$ for graphite anodes has limited the further development of LIBs, which require a high energy storage capability[2]. For sodium-ion batteries (SIBs), which are considered less expensive and safer candidates for energy storage than LIBs are, graphite is rarely used as an anode because of the larger ionic size of sodium ions (Na^+: 1.02 Å) than that of lithium ions (Li^+: 0.76 Å)[3] and the positive formation energy (~ 0.03 eV per atom for NaC_6) of Na–graphite compounds[4]. To improve the kinetics of Na^+ in the anode and the structural stability of the anode during sodiation/desodiation, porous carbons with good electrical conductivity and stable structures have received special attention as the focus of research for SIBs[5]. Moreover, porous carbons with a high specific surface area (SSA) can absorb more Li^+ and accelerate the diffusion of Li^+ in the anode, which further improves the specific capacity and rate performance to a level beyond that of graphite[6].

To obtain porous carbons, a wide range of precursors, such as biomass[7,8], resin[9,10] and rubber[11,12], have been used for physical processing (e.g., templated carbonization or direct laser drilling)[6,13] or chemical reactions (e.g., KOH activation or annealing in an NH_3 atmosphere)[14,15], but most porous carbons have a random distribution of pores and are thus vulnerable in terms of stability or reliability for use in LIBs or SIBs. Recently, fullerenes have been found to be rich in redox chemistry as anodes in batteries because of their excellent electron acceptance ability[16]. Specifically, the voids in the periodic molecular crystals made of fullerenes, such as the tetrahedral (d = 2.24 Å) and octahedral (d = 4.12 Å) sites in fcc C_{60} molecular crystals, can accommodate alkali metal atoms at evaluated temperatures (e.g., higher than 180 °C)[17] or under electrochemical conditions (e.g., in a Li||C_{60} half-cell with a $P(EO)_8LiClO_4$ polymer electrolyte working at 80 °C)[18]. By fully occupying all the void sites in the molecular crystals, i.e., 28 Li or 11 Na per C_{60} in the fcc lattice, a theoretical capacity of 1041.5 $mA \cdot h \cdot g^{-1}$ ($Li_{28}C_{60}$) or 409.2 $mA \cdot h \cdot g^{-1}$ ($Na_{11}C_{60}$) can be predicted[19,20], largely exceeding that of graphite.

However, with potential applications in energy storage, the fcc C_{60} molecular crystal has poor electrical conductivity (2.4 × 10^{-9} $S \cdot cm^{-1}$) and poor structural stability in organic electrolytes[16,21,22], which often requires reducing the dimensions of the C_{60} crystals or functionalizing C_{60} with chemical groups to stabilize the anode. For example, Yin et al. reported the preparation of nanoparticles composed of C_{60} arranged in a fcc structure by thermal evaporation[23]. When used as the anode

CSTR: 32290.14.JUSTC-2024-0115
DOI: 10.52396/JUSTC-2024-0115
JUSTC, **2026**, 55(X):

of LIBs, the C_{60} nanoparticles exhibited a capacity of 786 $mA{\cdot}h{\cdot}g^{-1}$ at 0.1 $A{\cdot}g^{-1}$. In another work, Shan et al. reported the preparation of carboxyl-, ester- or piperazine-functionalized C_{60} with well-defined molecular structures[24]. The C_{60} derivatives demonstrated specific capacities of 861, 404 or 83 $mA{\cdot}h{\cdot}g^{-1}$ measured in the 100th cycle at 0.1 C for carboxyl-, ester- or piperazine-functionalized C_{60}, respectively. In contrast, pristine C_{60} merely showed a capacity of 170 $mA{\cdot}h{\cdot}g^{-1}$ under the same testing conditions. To further improve electrical conductance, Tan et al. reported the preparation of nitrogen-doped porous carbon by treating a mixture of C_{60} and KOH at 700 °C in an atmosphere of NH_3 and Ar and demonstrated a reversible capacity of 1900 $mA{\cdot}h{\cdot}g^{-1}$ at 0.1 $mA{\cdot}g^{-1}$ as the anode of LIBs[14], but the cage structure of C_{60} in porous carbon was severely damaged. Novel carbons with better structural stability while maintaining the periodicity of C_{60} in the anode are extremely desirable. The storage of Na^+ in such carbons has yet to be explored.

In previous work, we fabricated a new carbon, long-range ordered porous carbon (denoted LOPC), by inducing covalent bonds between fcc C_{60} cages in a molecular crystal via electron injection from α-Li_3N at ambient pressure[21]. LOPC consists of sp^2-carbon-connected partially broken fcc C_{60} cages that maintain the long-range periodicity of the pristine C_{60} molecular crystal (called fcc C_{60} in the following discussion), but with a much higher SSA (327.1 $m^2{\cdot}g^{-1}$) and enhanced pore volume (0.099 $cm^3{\cdot}g^{-1}$) than those of the fcc C_{60} powder (SSA: 14.3 $m^2{\cdot}g^{-1}$, pore volume: 0.001 $cm^3{\cdot}g^{-1}$), as characterized in this work. As anodes of LIBs and SIBs, LOPC has a specific capacity of 820.9 $mA{\cdot}h{\cdot}g^{-1}$ in LIBs and 292.9 $mA{\cdot}h{\cdot}g^{-1}$ in SIBs, both of which were measured at a current density of 0.1 $A{\cdot}g^{-1}$. Kinetic analysis revealed that LOPC provides more capacitive storage of Na^+ than of Li^+, which may be related to the different ion radii and storage forms within the abundant ultramicropores of LOPC.

2 Experimental setup

2.1 Preparation of LOPC

A total of 500 mg of fcc C_{60} powder (Suzhou Dade Carbon Nanotechnology Co., Ltd., 99.5 at%, China) without any grinding was put into a quartz tube (closed at one end). Then, 250 mg of α-Li_3N powder (99.4 wt%, metal basis, 60 mesh, Alfa Aesar, USA) was added to the quartz tube (in a glovebox under an argon atmosphere with H_2O and O_2 concentrations below 0.01 ppm). The two powders were uniformly mixed by shaking in a quartz tube and then sealed at a high temperature under vacuum. Finally, the quartz tube with mixed powders was heated from room temperature to 520°C at a heating rate of $5°C{\cdot}min^{-1}$ under an argon flow of 100 sccm for 3 h to obtain long-range ordered porous carbon (LOPC).

2.2 Purification of LOPC

LOPC samples were washed in toluene via ultrasonic treatment and vacuum filtration to remove unreacted fcc C_{60}. The residual toluene was subsequently removed with ethanol, and α-Li_3N and $LiCO_3$ were removed via diluted hydrochloric acid and deionized water via ultrasonic treatment and vacuum filtration until the filtrate became colorless and neutral. The obtained samples were dried at 60 °C in air for 12 h.

2.3 Characterization of LOPC

The samples were evaluated via Raman spectroscopy (LabRAM, RM3000, Renishaw, UK, 532 nm laser) and X-ray diffraction (XRD) with Cu Kα radiation (λ = 1.5418 Å, tube voltage 40 kV, tube current 30 mA, Rigaku SmartLab, Japan). The morphology of the samples was characterized via SEM (Hitachi, SU8200, Japan) and HR-TEM (JEOL-2100F, Japan).

2.4 Fabrication of half-cells

For the fabrication of the anodes, 60 wt% active material (LOPC) was mixed with 30 wt% Ketjenblack (EC-600JD, Li-on Corporation) and 10 wt% polyvinyl fluoride (PVDF) and dispersed in N-methyl-2-pyrrolidone (NMP) to form a slurry. The slurry was spread and pressed on a carbon-coated copper foil and dried at 80 °C for 12 h under vacuum. The active material with a mass loading of 1.5~2.0 $mg{\cdot}cm^{-2}$ was punched into round electrodes with a diameter of 10 mm. For Li^+ or Na^+ half-cells, 2032-type coin half-cells were assembled in an argon-filled glove box (H_2O and O_2 concentrations below 0.01 ppm), using Li or Na foil simultaneously as the reference and counter electrode, 1.0 M lithium hexafluorophosphate ($LiPF_6$) in ethylene carbonate (EC):diethyl carbonate (DEC)=1:1 Vol% with 5% fluoroethylene carbonate (FEC) or 1.0 M $NaPF_6$ in diethylene glycol dimethyl ether (DEGDME) as the electrolyte, and glass fiber as the separator.

2.5 Electrochemical measurements

Cyclic voltammetry (CV) from 0.001 V to 2.5 V (vs. Na/Na^+) or 3.0 V (vs. Li/Li^+) at various scanning rates and electrochemical impedance spectroscopy (EIS) measurements at a frequency of ± 5 mV were performed on a PARSTAT MC electrochemical workstation (Princeton Company, USA). Galvanostatic charge–discharge (GCD) measurements at various current densities and cycle stability tests for half-cells and full cells were conducted on a Neware battery testing system (CT-4008T, Shenzhen, China). The weight was based on the active materials (LOPC), excluding Ketjenblack and PVDF.

3 Results and discussion

3.1 Materials characterization

Under ambient conditions, fcc C_{60} can form a molecular crystal with the space group *Fm-3 m*, as shown by the (111), (220) and (311) diffraction peaks in the X-ray diffraction (XRD) pattern in Fig. 1a. After annealing with α-Li_3N at 520 °C for 3 h followed by cleaning, the LOPC obtained shows broader (111), (220) and (311) XRD peaks. The widening of the diffraction peaks and bulging of the background indicate a decrease in crystallinity caused by grain fragmentation and disordered covalent bond connections between partially broken C_{60} molecules[21], but the unchanged positions of the main peaks suggest that the LOPC maintains the fcc stacking of the original molecular crystal. Moreover, the intensity of the (111) diffraction peak is significantly weakened. The (222) diffraction peak is the second-order diffraction peak of

CSTR: 32290.14.JUSTC-2024-0115
DOI: 10.52396/JUSTC-2024-0115
JUSTC, **2026**, 55(X):

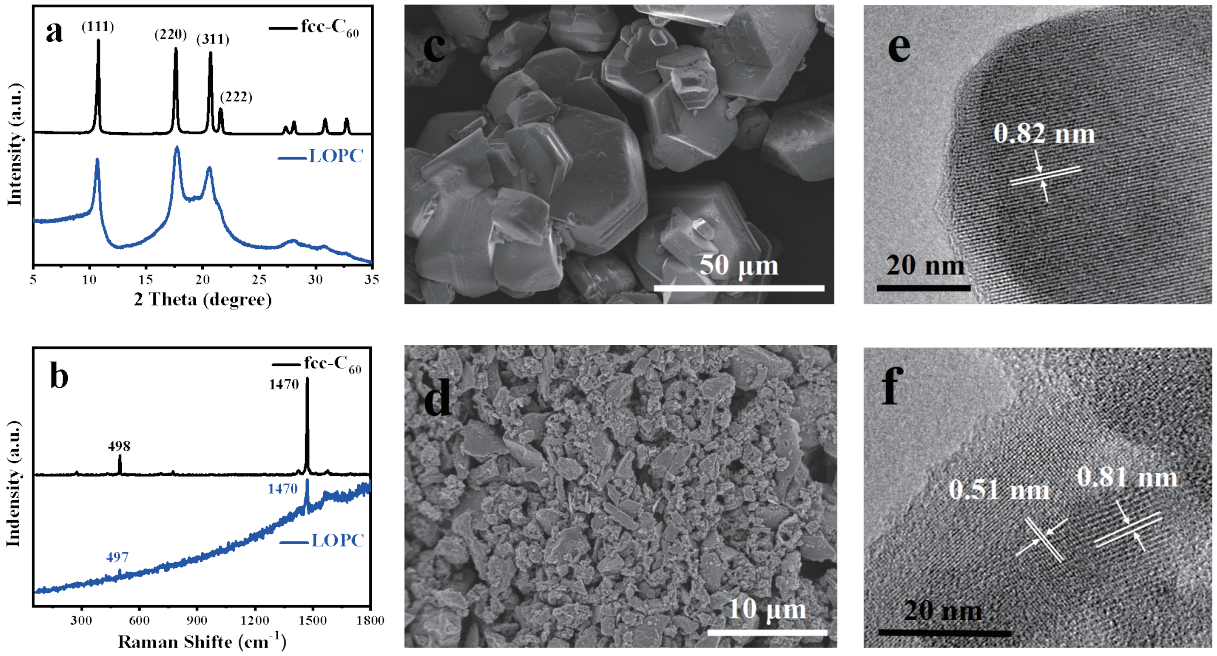

Fig. 1. (a) XRD patterns; (b) Raman spectra, SEM images and TEM images of (c, e) fcc C_{60} and (d, f) LOPC.

(111), and the intensity is generally weak. When the intensity of the (111) diffraction peak is weakened, the intensity of the (222) diffraction peak further weakens or even disappears. In addition, the intensities of the (331), (420), (422) and (511) diffraction peaks are weakened or disappear because of the destruction of the lattice planes in the fcc-C_{60} crystal after the intense reaction. The Raman spectra in Fig. 1b show the typical Ag(1) and Ag(2) peaks of fcc C_{60} molecules at 498 cm^{-1} and 1470 cm^{-1}, respectively, which are characteristic peaks of fcc C_{60} molecules due to their high symmetry[25]. In comparison, LOPC exhibits two weakened Raman peaks located at 497 cm^{-1} and 1470 cm^{-1}, which can be explained by the formation of covalent bonds between C_{60} molecules and reduced symmetry[26,27]. The scanning electron microscopy (SEM) image of the fcc C_{60} crystal (Fig. 1c) shows particles with hexagonal edges and smooth surfaces. After annealing with α-Li_3N and further purification to remove α-Li_3N or other residues, LOPC (Fig. 1d) shows fragmented blocks with much rougher surfaces. The structures of fcc C_{60} and LOPC were further identified via high-resolution transmission electron microscopy (HRTEM), as shown in Fig. 1e, f. The labeled spacing in Fig. 1e is attributed to the (111) crystal plane in fcc C_{60}, whereas the ordered lattice fringes in the magnified HRTEM image (Fig. 1f) are measured to be ca. 0.51 and 0.81 nm, corresponding to the (220) and (111) interlayer spacings of LOPC, respectively, indicating that LOPC has a periodic structure, which is in accordance with the XRD results.

Nitrogen (N_2) adsorption at 77 K is used to measure the SSA, pore size distribution, and pore volume of mesoporous solids, whereas carbon dioxide (CO_2) adsorption at 273.2 K is used to assess ultramicropores because of the accessibility of CO_2 to smaller pores[28,29]. Owing to the periodic arrangement of covalently connected (partially broken) fcc C_{60} cages, the pores formed by the gaps between C_{60} are likely to also be periodically distributed. Fig. 2a shows a proposed structure of LOPC, which was previously obtained by comprehensively comparing the structural characterizations and theoretical modeling results[21]. The distances in the voids between periodical broken fcc C_{60} are labeled as references. The N_2 isothermal adsorption/desorption and CO_2 isothermal adsorption results are shown in Fig. 2b, c. We can see that the N_2 or CO_2 adsorption quantity of LOPC is much greater than that of fcc C_{60}. The SSA measured by N_2 or CO_2 adsorption is 97.8 $m^2 \cdot g^{-1}$ or 327.1 $m^2 \cdot g^{-1}$ for LOPC, much higher than 0.63 $m^2 \cdot g^{-1}$ or 14.3 $m^2 \cdot g^{-1}$ for fcc C_{60}. From the pore size distribution shown in Fig. 2d, we can see that LOPC has a wide distribution of micro- or mesopores with widths peaking at ~ 1.5, ~ 3 and ~ 6 nm, as measured by N_2 adsorption. Essentially, the original fcc C_{60} sample has a small peak at ~ 4.5 nm, corresponding to the very small volume of 0.001 $cm^3 \cdot g^{-1}$. A comparison of the data in Fig. 2d and e reveals that LOPC is rich in ultramicropores in the range of 0.3--0.75 nm, as measured by CO_2 adsorption, corresponding to a 19-fold increase in ultramicropore volume from 0.005 $cm^3 \cdot g^{-1}$ for fcc C_{60} to 0.095 $cm^3 \cdot g^{-1}$ for LOPC. Referring to the structure shown in Fig. 2a, the rich micropores or ultramicropores in LOPC may be attributed to the more cavities formed and defects formed between broken C_{60} cages, whereas fcc C_{60} is limited by the close cage, resulting in a limited pore volume measured by gas adsorption.

3.2 Electrochemical performance measurements

To evaluate the Li^+ and Na^+ storage performance of LOPC, Li||LOPC or Na||LOPC half-cells were assembled with 1.0 M lithium hexafluorophosphate ($LiPF_6$) in EC:DEC (1:1 Vol.%) with 5% FEC or 1.0 M sodium hexafluorophosphate ($NaPF_6$) in DEGDME as the electrolyte, and the results are shown in Fig. 3. Fig. 3a, b shows the corresponding charge/discharge profiles of Li^+ or Na^+ storage in LOPCs during the first 3 cycles at 0.1 $A \cdot g^{-1}$, which both show slope-dominated curves. The first discharge specific capacity of Li^+ storage is 1612.9

CSTR: 32290.14.JUSTC-2024-0115
DOI: 10.52396/JUSTC-2024-0115
JUSTC, **2026**, 55(X):

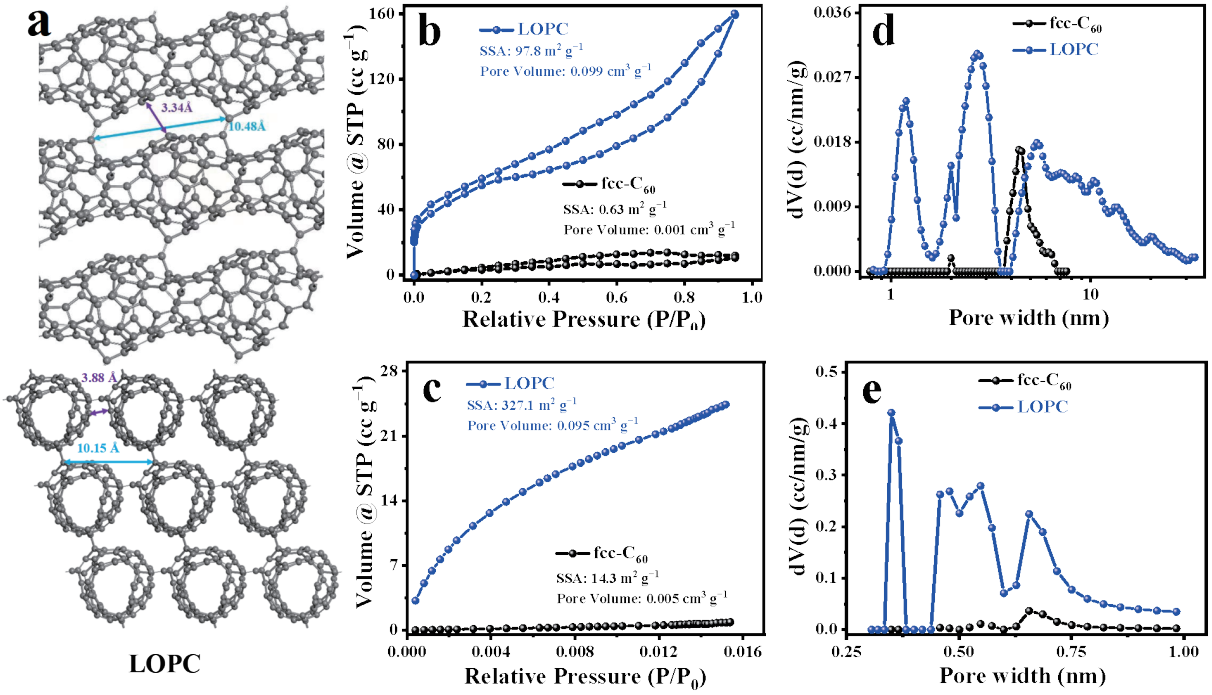

Fig. 2. (a) Proposed structure of LOPC. (b) N_2 isothermal adsorption/desorption and (c) CO_2 isothermal adsorption curves of fcc C_{60} and LOPC. Pore size distribution (NLDFT equilibrium model) from (d) N_2 and (e) CO_2 measurements.

mA·h·g^{-1}, and the charge specific capacity is 664.1 mA·h·g^{-1}, corresponding to an initial Coulombic efficiency (ICE) of 41.2%. The first discharge specific capacity of Na^+ storage is 556.5 mA·h·g^{-1}, and the charge specific capacity is 367.1 mA·h·g^{-1}, corresponding to an ICE of 65.9%. The SSA of LOPC might cause massive solid–electrolyte interphase (SEI) formation and electrolyte decomposition, resulting in a low ICE. However, such an SEI film can significantly inhibit Li/Na dendrite formation, thus achieving high safety performance[30]. On the other hand, the high SSA provides many active sites for Na^+ or Li^+ adsorption, which explains the sloping region during charging and discharging[31].

As shown in Fig. 3c, d, the adsorption-based storage enables the LOPC to exhibit an impressive rate performance in Li^+ and Na^+ storage, especially in Na^+ storage. Compared with the capacity retention of 35.4% (1180.9 mA·h·g^{-1} at 0.01 A·g^{-1} to 417.8 mA·h·g^{-1} at 1.0 A·g^{-1}) for the LOPC anode in LIBs, the LOPC shows a capacity retention of 49.0% in the SIB when the current density is increased from 0.1 A g^{-1} (292.9 mA·h·g^{-1}) to 10.0 A·g^{-1} (143.4 mA·h·g^{-1}). LOPC has a specific capacity of 820.9 mA·h·g^{-1} or 292.9 mA·h·g^{-1} as an anode for LIBs or SIBs, both of which are measured at a current density of 0.1 A·g^{-1}, whereas the current density from 1.0 A·g^{-1} or 10.0 A·g^{-1} recovers to 0.1 A·g^{-1}. The specific capacity for LIBs or SIBs returns to 713.7 mA·h·g^{-1} or 239.1 mA·h·g^{-1}, indicating that the electrode has good reversibility of charge and discharge. The superior rate performance of LOPC in SIBs may be related to the open pores and the 'cointercalation' of solvated Na^+ in the ether-based electrolyte during discharge[32]. The long cycling performance was evaluated at 1.0 A·g^{-1}, and the results are shown in Fig. 3e, f. After 200 cycles, the LOPC as the anode of the LIBs remained at 359.8 mA·h·g^{-1}, corresponding to a capacity retention of 68.5% (related to 525.3 mA·h·g^{-1} in the 2nd cycle). The LOPC remains at 190.1 mA·h·g^{-1} in the SIBs, corresponding to a capacity retention of 70.4% (related to 270.1 mA·h·g^{-1} in the 2nd cycle). After 450 cycles, the specific capacities of the LIBs and SIBs are 223.6 mA·h·g^{-1} and 128.4 mA·h·g^{-1}, corresponding to Coulombic efficiencies of 99.1% and 100.4%, respectively.

To better understand Li^+ and Na^+ storage, the ionic transport of LOPC was evaluated via electrochemical impedance spectroscopy (EIS). The fitting based on the equivalent circuit diagram gives an R_{ct} value of 251.9 Ω for the Li half-cell (Fig. 4a) and 57.5 Ω for the Na half-cell (Fig. 4b) on the basis of the LOPC. Generally, a low R_{ct} promotes the rapid transfer of electrons during the reaction, which usually leads to improved rate performance for Na^+ storage. The higher conductivity (3.8×10^{-5} S·cm^{-1} for LOPC vs. 2.4×10^{-9} S·cm^{-1} for fcc C_{60}) may be related to greater delocalization of the electrons in the LOPC structure. The shape of the cyclic voltammetry (CV) curves for the half-cells is well preserved as the scan rates increase, as shown in Fig. 4c, d. Fig. 4c shows a broad cathodic peak at approximately 0.77 V (vs. Li/Li^+) and a clear cathodic peak at 0.01 V (vs. Li/Li^+), whereas Fig. 4d shows three clear cathodic peaks at 1.20 V, 0.43 V and 0.05 V (vs. Na/Na^+). The peaks in Fig. 4c shift to lower potentials upon scanning, which are probably affected by the increase in polarization, whereas the peak positions in Fig. 4d remain nearly unchanged. The different Li^+ and Na^+ storage behaviors in the CV curves may be due to their different ion radii and electronic properties, especially when they enter the pores of LOPCs.

On the basis of the scan rate (v) and peak current (i), the slope b of the log (v) vs log (i) curves can be calculated according to the equation $i = av^b$ [33]. A b value of 0.5 refers to a semi-infinite diffusion process, and b = 1 indicates surface-controlled or capacitor-like kinetics. For the Li^+ storage pro-

CSTR: 32290.14.JUSTC-2024-0115
DOI: 10.52396/JUSTC-2024-0115
JUSTC, **2026**, 55(X):

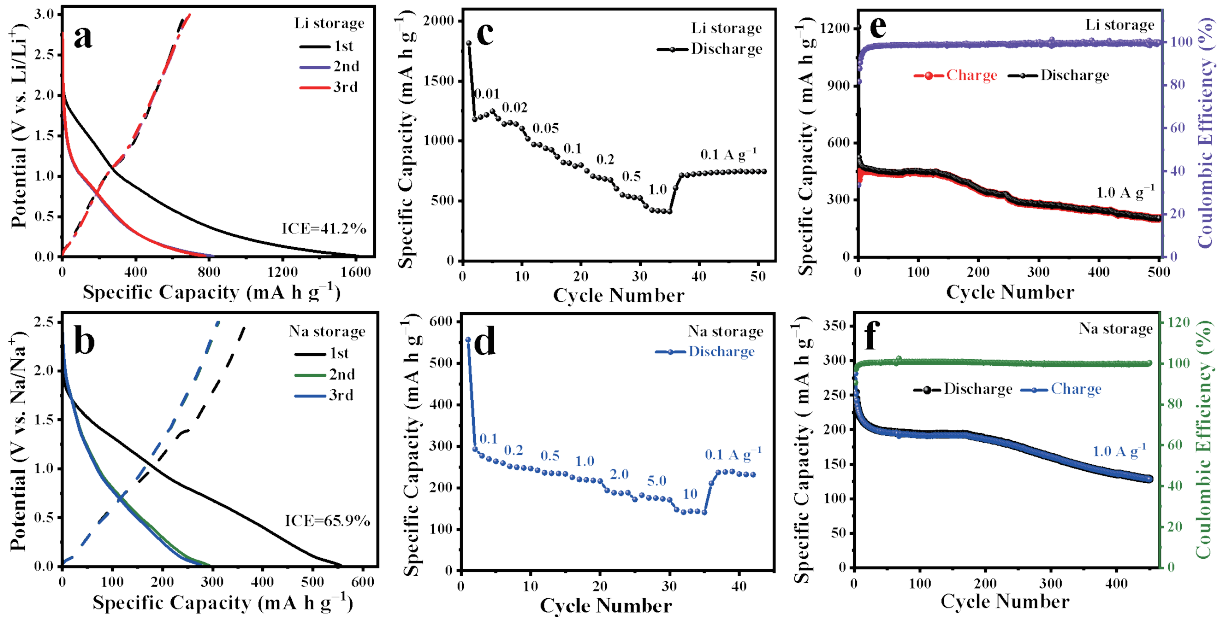

Fig. 3. Electrochemical evaluation of the LOPC for Li^+ and Na^+ storage. (a, b) Charge–discharge curves of the first 3 cycles at 0.1 $A \cdot g^{-1}$. Rate performances measured (c) from 0.01 to 1.0 $A \cdot g^{-1}$ for Li^+ storage and (d) from 0.1 $A \cdot g^{-1}$ to 10.0 $A \cdot g^{-1}$ for Na^+ storage. (e, f) Long-term cycling performance and Coulombic efficiency measured at a current density of 1.0 $A \cdot g^{-1}$.

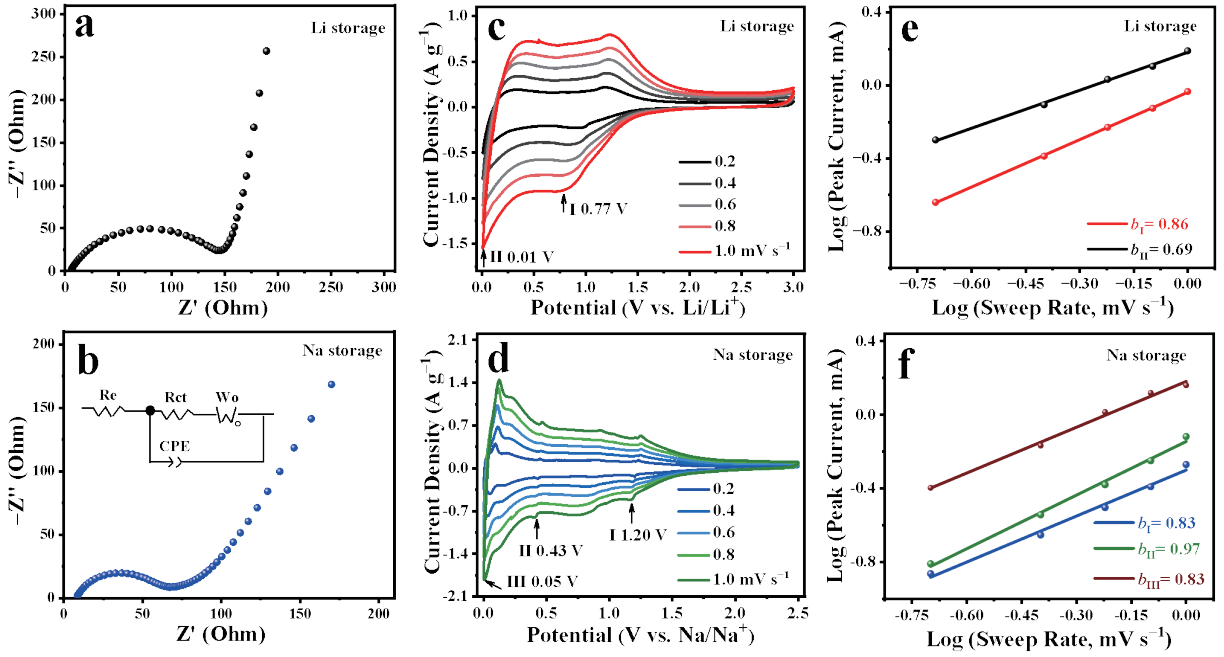

Fig. 4. Kinetic analysis of the LOPC for lithium and sodium half-cells. (a, b) Nyquist plots (insert: equivalent circuit diagram). (c, d) CV curves at different scan rates from 0.2 to 1.0 $mV \cdot s^{-1}$. (e, f) Determination of the b values in the cathodic peak region.

cess, the *b* value of Peak Ⅰ (indicated in Fig. 4e of the red line) is 0.86, suggesting a diffusion-controlled and/or pseudocapacitive controlled process. The *b* value of Peak II is 0.69, indicating a more diffusion-controlled process when the voltage is lower than 0.1 V, as shown in Fig. 4e. Compared with those for Li^+ storage, the *b* values (from peaks Ⅰ, Ⅱ and Ⅲ shown in Fig. 4d) for Na^+ storage are 0.83, 0.97 and 0.83, implying that the Na^+ storage of LOPC is more dominated by the capacitive process, as shown in Fig. 4f. The difference in the kinetic behavior of Li^+ and Na^+ stored in LOPC may be due to the different ionic radii of Li^+ and Na^+, as the larger ionic radius of Na^+ may hinder their diffusion in LOPC materials, leading to more surface-controlled behavior. However, the different solvation structures of Li^+ and Na^+ due to electrolyte selection may affect their kinetic behavior[34]. In addition, the different SEIs formed on the surface of LOPC may also affect ion transport between interfaces or through pores[35,36], which requires further research.

4 Conclusions

In summary, long-range ordered carbon with distorted fcc symmetry has been explored as an anode material for LIBs

CSTR: 32290.14.JUSTC-2024-0115
DOI: 10.52396/JUSTC-2024-0115
JUSTC, **2026**, 55(X):

and SIBs. The sp^2 bonding was induced between C_{60} molecules, which significantly improved the chemical stability and electrical conductivity (3.8×10^{-5} S·cm^{-1} for LOPC vs. 2.4×10^{-9} S·cm^{-1} for fcc C_{60}). With more gaps between C_{60} cages and more defects, the SSA and pore volume of LOPC significantly increase. As the anode for Li^+ or Na^+ storage, LOPC has a specific capacity of 820.9 mA·h·g^{-1} for LIBs and 292.9 mA·h·g^{-1} for SIBs measured at a current density of 0.1 A·g^{-1}; the Li^+ or Na^+ storage capacity of the LOPC anode still remains at 359.8 mA·h·g^{-1} or 190.1 mA·h·g^{-1} after 200 cycles at 1.0 A·g^{-1}, corresponding to capacity retentions of 68.5% and 70.4%, respectively. After 450 cycles, the specific capacities of the LIBs and SIBs are 223.6 mA·h·g^{-1} and 128.4 mA·h·g^{-1}, corresponding to Coulombic efficiencies of 99.1% and 100.4%, respectively. Due to the high SSA and abundant ultramicropores of LOPC, both Li^+ and Na^+ exhibit adsorption-based storage behavior and no obvious discharge plateau. Especially at low voltages, SIBs exhibit more surface-controlled behavior than do LIBs. The highly ordered yet porous structure of LOPC may provide new opportunities for finely tuning the storage behavior of metallic ions in future high-performance anodes.

Acknowledgements

This work is supported by the National Key R&D Program of China (2020YFA0711502) and the National Natural Science Foundation of China (51972299, 52003265, 52202052, 52273234, 52273239, 52373310). F.P. is supported by the Xiaomi Young Talents Program.

Conflict of interest

The authors declare that they have no conflict of interest.

Biographies

Shengyuan Li is a PhD candidate under the supervision of Prof. Yanwu Zhu at the University of Science and Technology of China. His research interests focus on the synthesis of novel carbon nanomaterials and their applications for energy storage and conversion.

Yizhe Wang is currently a PhD candidate at the Hefei National Research Center for Physical Sciences at the Microscale, University of Science and Technology of China, under the supervision of Prof. Yanwu Zhu. His research interests focus on the mechanism and modification of the carbon material electrode/electrolyte interface for energy storage applications.

Fei Pan joined the University of Science and Technology of China as an associate research fellow in 2022. Before this, he received his PhD degree from the University of Science and Technology of China in 2020 under the supervision of Prof. Yanwu Zhu. He subsequently worked as a postdoctoral fellow at the University of Science and Technology of China. His current research interest is the synthesis of novel carbon materials and their properties.

Yanwu Zhu joined the University of Science and Technology of China as a full professor in 2011. Prior to this, he obtained his PhD degree in physics from the National University of Singapore in 2007. Then, he worked as a postdoctoral fellow sequentially at the National University of Singapore and at the University of Texas at Austin. His current research interest is the synthesis of novel carbon nanomaterials and their applications for energy storage and conversion.

References

[1] Quilty C D, Wu D, Li W, et al. Electron and ion transport in lithium and lithium-ion battery negative and positive composite electrodes. *Chemical Reviews*, **2023**, *123* (4): 1327–1363.
[2] Tarascon J M, Armand M. Issues and challenges facing rechargeable lithium batteries. *Nature*, **2001**, *414*: 359–367.
[3] Pan Q C, Zhang Q B, Zheng F H, et al. Construction of MoS_2/C hierarchical tubular heterostructures for high-performance sodium ion batteries. *ACS Nano*, **2018**, *12* (12): 12578–12586.
[4] Liu Y, Merinov B V, Goddard W A 3rd. Origin of low sodium capacity in graphite and generally weak substrate binding of Na and Mg among alkali and alkaline earth metals. *Proceedings of the National Academy of Sciences of the United States of America*, **2016**, *113* (14): 3735–3739.
[5] Xia J L, Yan D, Guo L P, et al. Hard carbon nanosheets with uniform ultramicropores and accessible functional groups showing high realistic capacity and superior rate performance for sodium-ion storage. *Advanced Materials*, **2020**, *32* (31): e2000447.
[6] Zhao Z, Das S, Xing G, et al. A 3D organically synthesized porous carbon material for lithium-ion batteries. *Angewandte Chemie International Edition*, **2018**, *57* (37): 11952–11956.
[7] Szczęśniak B, Phuriragpitikhon J, Choma J, et al. Recent advances in the development and applications of biomass-derived carbons with uniform porosity. *Journal of Materials Chemistry A*, **2020**, *8* (36): 18464–18491.
[8] Zhang Y, Liu S S, Zheng X Y, et al. Biomass organs control the porosity of their pyrolyzed carbon. *Advanced Functional Materials*, **2017**, *27* (3): 1604687.
[9] Wei Z, Zhao H X, Niu Y B, et al. Insights into the pre-oxidation process of phenolic resin-based hard carbon for sodium storage. *Materials Chemistry Frontiers*, **2021**, *5* (10): 3911–3917.
[10] Fan C L, Zhang R S, Luo X H, et al. Epoxy phenol novolac resin: A novel precursor to construct high performance hard carbon anode toward enhanced sodium-ion batteries. *Carbon*, **2023**, *205*: 353–364.
[11] Wu Z Y, Ma C, Bai Y L, et al. Rubber-based carbon electrode materials derived from dumped tires for efficient sodium-ion storage. *Dalton Transactions*, **2018**, *47* (14): 4885–4892.
[12] Li Y, Paranthaman M P, Akato K, et al. Tire-derived carbon composite anodes for sodium-ion batteries. *Journal of Power Sources*, **2016**, *316* (1): 232–238.
[13] Qu W D, Zhao Z Z, Wang J, et al. Direct laser writing of pure lignin on carbon cloth for highly flexible supercapacitors with enhanced areal capacitance. *Sustainable Energy & Fuels*, **2021**, *5* (14): 3744–3754.
[14] Tan Z Q, Ni K, Chen G X, et al. Incorporating pyrrolic and pyridinic nitrogen into a porous carbon made from C_{60} molecules to obtain superior energy storage. *Advanced Materials*, **2017**, *29* (8): 1603414.
[15] Li S Y, Yuan H, Ye C R, et al. Sucrose-derived hard carbon wrapped with reduced graphene oxide as a high-performance anode for sodium-ion batteries. *Journal of Materials Chemistry A*, **2023**, *11* (18): 9816–9823.
[16] Jiang Z P, Zhao Y M, Lu X, et al. Fullerenes for rechargeable battery applications: Recent developments and future perspectives. *Journal of Energy Chemistry*, **2021**, *55* (5): 70–79.
[17] Haddon C, Hebard A, Rosseinsky M, et al. Conducting films of C_{60} and C_{70} by alkali-metal doping. *Nature*, **1991**, *350*: 320–322.
[18] Chabre Y, Djurado D, Armand M, et al. Electrochemical intercalation of lithium into solid fullerene C_{60}. *Journal of the American Chemical Society*, **1992**, *114* (2): 764–766.
[19] Yasukawa M, Yamanaka S. Synthesis of Li_xC_{60} (x=1–28) fullerides under high-pressure and high-temperature conditions and their electrical properties. *Chemical Physics Letters*, **2001**, *341*: 467–475.

CSTR: 32290.14.JUSTC-2024-0115
DOI: 10.52396/JUSTC-2024-0115
JUSTC, **2026**, 55(X):

[20] Yildirim T, Zhou O, Fischer J E, et al. Intercalation of sodium heteroclusters into the C_{60} lattice. *Nature*, **1992**, *360*: 568–571.
[21] Pan F, Ni K, Xu T, et al. Long-range ordered porous carbons produced from C_{60}. *Nature*, **2023**, *614*: 95–101.
[22] Seger L, Wen L Q, Schlenoff J B. Prospects for using C_{60} and C_{70} in lithium batteries. *Journal of The Electrochemical Society*, **1991**, *138* (12): L81.
[23] Yin L, Cho J, Kim S J, et al. Abnormally high - lithium storage in pure crystalline C_{60} nanoparticles. *Advanced Materials*, **2021**, *33* (43): 2104763.
[24] Shan C, Yen H J, Wu K, et al. Functionalized fullerenes for highly efficient lithium ion storage: Structure-property-performance correlation with energy implications. *Nano Energy*, **2017**, *40*: 327–335.
[25] Adams G B, Page J B, Sankey O F, et al. First-principles quantum molecular-dynamics study of the vibrations of icosahedral C_{60}. *Physical Review B*, **1991**, *44* (8): 4052–4055.
[26] Yamawaki H, Yoshida M, Kakudate Y, et al. Infrared study of vibrational property and polymerization of fullerene C_{60} and C_{70} under pressure. *The Journal of Physical Chemistry*, **1993**, *97* (43): 11161–11163.
[27] Davydov V A, Kashevarova L S, Rakhmanina A V, et al. Spectroscopic study of pressure-polymerized phases of C_{60}. *Physical Review B*, **2000**, *61* (18): 11936–11945.
[28] Huang B, Bartholomew C H, Woodfield B F. Improved calculations of pore size distribution for relatively large, irregular slit-shaped mesopore structure. *Microporous and Mesoporous Materials*, **2014**, *184*: 112–121.
[29] Zhu Y W, Murali S, Stoller M D, et al. Carbon-based supercapacitors produced by activation of graphene. *Science*, **2011**, *332* (6037): 1537–1541.
[30] Chan C K, Ruffo R, Hong S S, et al. Surface chemistry and morphology of the solid electrolyte interphase on silicon nanowire lithium-ion battery anodes. *Journal of Power Sources*, **2009**, *189* (2): 1132–1140.
[31] Zhao L F, Hu Z, Lai W H, et al. Hard carbon anodes: Fundamental understanding and commercial perspectives for Na-ion batteries beyond Li-ion and K-ion counterparts. *Advanced Energy Materials*, **2021**, *11* (1): 2002704.
[32] Li Y, Wu F, Li Y, et al. Ether-based electrolytes for sodium ion batteries. *Chemical Society Reviews*, **2022**, *51* (11): 4484–4536.
[33] Lu P, Sun Y, Xiang H F, et al. 3D amorphous carbon with controlled porous and disordered structures as a high-rate anode material for sodium-ion batteries. *Advanced Energy Materials*, **2018**, *8* (8): 1702434.
[34] Ho J S, Borodin O A, Ding M S, et al. Understanding lithium-ion transport in sulfolane- and tetraglyme-based electrolytes using very low-frequency impedance spectroscopy. *Energy & Environmental Materials*, **2023**, *6* (1): e12302.
[35] Ji X, Zhang J Q. Strain effects on Li^+ diffusion in solid electrolyte interphases: A molecular dynamics study. *Chinese Physics B*, **2023**, *32* (6): 066601.
[36] Li Q, Liu X S, Tao Y, et al. Sieving carbons promise practical anodes with extensible low-potential plateaus for sodium batteries. *National Science Review*, **2022**, *9* (8): nwac084.

CSTR: 32290.14.JUSTC-2024-0115
DOI: 10.52396/JUSTC-2024-0115
JUSTC, **2026**, 55(X):